

Tetrapropyl-tetraphenyl-diindenoperylene derivative as a green absorber for high-voltage stable organic solar cells

Jan Meiss,¹ Martin Hermenau,¹ Wolfgang Tress,¹ Christoph Schuenemann,¹ Franz Selzer,¹ Markus Hummert,¹ Joerg Alex,¹ Gerhard Lackner,² Karl Leo,¹ and Moritz Riede^{1,*}

¹*Institut für Angewandte Photophysik, Technische Universität Dresden, D-01062 Dresden, Germany*

²*Institut für Materialwissenschaft, Fakultät Ingenieurwissenschaften, Universität Duisburg-Essen, Campus Essen, D-45117 Essen, Germany*

(Received 20 December 2010; published 11 April 2011)

We present small molecule organic solar cells (SMOSC) based on flat heterojunctions (FHJ) of the alternative green donor 2,3,10,11-tetrapropyl-1,4,9,12-tetraphenyl-diindeno[1,2,3-cd:1',2',3'-lm]perylene (P4-Ph4-DIP) and the fullerene C₆₀. P4-Ph4-DIP absorbs in the green spectral range and thus fills the spectral gap that standard absorber materials (zinc or copper phthalocyanine for red and C₆₀ for blue absorption) leave, thus allowing broad coverage of the sun spectrum, which is of major interest for tandem devices. The materials properties of P4-Ph4-DIP are studied, and SMOSC are characterized by current voltage, external quantum efficiency, and aging measurements. The solar cells display very high fill factors FF > 76% and open circuit voltages V_{OC} of close to 1 V. Mismatch-corrected efficiencies of up to 1.9% are obtained. Aging measurements show that C₆₀ in conjunction with P4-Ph4-DIP yields extremely stable devices. We observe ≈ 88% of the initial efficiency after 2500 h illumination at 999 mW/cm² illumination intensity, with no observable change in short-circuit current density. Furthermore, we also show that a systematic variation of donor thickness in FHJ can be combined with transfer matrix formalism-based optical simulations and the continuity equation for excitons to reliably determine the exciton diffusion length L_D. A value of 9 ± 1 nm is found for P4-Ph4-DIP.

DOI: [10.1103/PhysRevB.83.165305](https://doi.org/10.1103/PhysRevB.83.165305)

PACS number(s): 88.40.jr, 33.90.+h, 68.55.-a, 81.05.Fb

I. INTRODUCTION

The field of organic photovoltaics (OPV) has attracted considerable interest as a potential cost-efficient technology to generate electrical power. New materials and concepts have resulted in certified efficiencies of 8.3% for small molecule organic solar cells (SMOSC),¹ and recently also 8.3% for polymer devices.² The field of OPV provides a unique opportunity for joint research activities of materials scientists, device physicists, and organic chemists alike, and new materials play a decisive role in extending power conversion efficiency and physical understanding.

Currently, copper or zinc phthalocyanine (CuPc and ZnPc) are used as standard donor materials with absorption in the red at wavelengths $\lambda > 600$ nm, often with the fullerene C₆₀ as blue-absorbing acceptor. However, such devices are limited by a low open circuit voltage V_{OC} < 0.55 V and fill factors FF < 60%;³⁻⁹ furthermore, since such combinations of phthalocyanine and C₆₀ absorb only in the red and blue range of the solar spectrum, there is a large gap in the green between 500–600 nm where only little absorption is observed.¹⁰

We investigate here an attractive candidate to fill this gap, the material 2,3,10,11-tetrapropyl-1,4,9,12-tetraphenyl-diindeno[1,2,3-cd:1',2',3'-lm]perylene (P4-Ph4-DIP) which can be used as green donor.¹¹ The optical constants and the molecular structure of P4-Ph4-DIP are shown in Fig. 1, together with the extinction coefficient of C₆₀. The absorption spectrum exhibits maxima in the green, making P4-Ph4-DIP an ideal material to fill the gap in tandem devices for complementary absorption if combined with adequate blue and red absorbers.

In this contribution, we show that the energy levels of P4-Ph4-DIP are very suitable for utilization with C₆₀ as acceptor, resulting in high V_{OC}, and that very high FF can be achieved. By using flat heterojunction (FHJ) solar cell devices and a

systematic parameter variation to gain a large data set and solving the continuity equation for excitons, we determine the exciton diffusion length L_D. Lifetime measurements document that extremely stable SMOSC can be created that retain ≈ 90% of their initial power conversion efficiency η after 2500 h of constant illumination at 999 mW/cm² intensity.

II. EXPERIMENTAL METHODS

For device fabrication, we use a custom-made vacuum system (K.J. Lesker, UK) at a base pressure of 10⁻⁸ mbar, with shadow masks. Indium-tin oxide coated glass (TFD, USA) with a sheet resistance of 30 Ω /sq, pretreated with acetone, ethanol, and oxygen plasma is used as substrate. 24 samples are made on the same substrate in one run, ensuring reproducible and comparable conditions for all layers and allowing for intentional variation of only single layers or parameters, in this case the layer thickness of P4-Ph4-DIP.

The SMOSC in the present work are *n-i-p* type, i.e., the intrinsic absorber (i) is embedded between dedicated electron (n) and hole (p) transport materials; the complete stack is shown in Fig. 1. As n-type material, 5 nm of n-doped C₆₀ is used. 25 nm intrinsic C₆₀ serves as acceptor material. A flat heterojunction (FHJ) is formed between the fullerene and the subsequently deposited P4-Ph4-DIP (0–66 nm thickness). For efficient hole transport, we use 40 nm BPAPF doped with 20 wt% NDP9 (Novaled AG, Dresden, Germany),¹² followed by 10 nm 10 wt% p-doped ZnPc. Good hole extraction is achieved by 4 nm Au and 100 nm Al as back electrode. All organic materials except the dopant had been purified at least twice by vacuum gradient sublimation.

The completed solar cells are encapsulated with a transparent encapsulation glass, fixed by UV-hardened epoxy glue, in a nitrogen glove box attached directly to the vacuum deposition

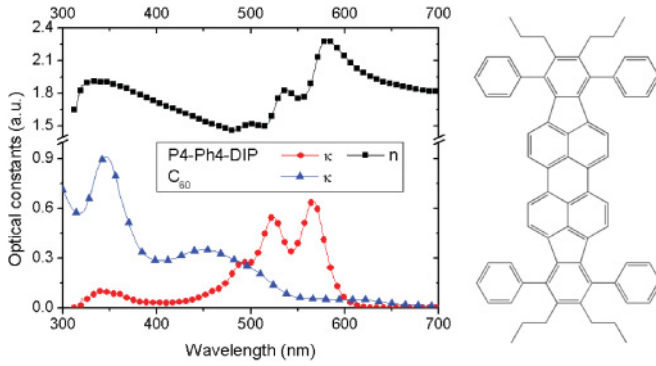


FIG. 1. (Color online) Left: optical constants n and κ , as determined from transmittance and reflectance measurements. Right: molecular structure of P4-Ph4-DIP: a diindenoperylene core with four phenyl rings and four propyl chains as substituents.

chamber. Moisture getter sheets (Dynic Ltd., PRC) are used in a cavity of the cover glass to prevent device degradation. The finished SMOSC are stored at ambient conditions. Typical solar cell active areas, defined by the overlap of ITO and metal back contact, are around 6.18 mm^2 (measured using a light microscope).

Current voltage characteristics are recorded using a source measurement unit (Keithley) under an AM 1.5G sun simulator SC1200 (KHS Technical Lighting, Germany), monitored with a Hamamatsu S1337 silicon photodiode (calibrated by Fraunhofer ISE) with respect to which intensities are measured. The reported efficiency values are corrected for spectral mismatch. The values for $J_{SC, \text{norm}}$ represent the measured short-circuit current densities, normalized to 100 mW/cm^2 using the mismatch corrected illumination intensities for better comparison.

External quantum efficiency (EQE) is measured employing lock-in techniques (signal recovery SR 7265 lock-in amplifier), in a custom-made setup with Xe illumination and a Newport Oriel Apex monochromator illuminator. The samples are measured through a photomask having an aperture of 2.958 mm^2 . Reflection and transmission measurements are performed on a Lambda 900 UV/VIS/NIR spectrometer (Perkin Elmer).

The optical simulations are performed using a numerical code based on the transfer matrix approach. This technique uses refractive index n , extinction coefficient κ (obtained from reflection and transmission measurements¹³), and the layer thickness to calculate, e.g., photon absorption, short-circuit current, and distribution of the optical field within the solar cell. The model is purely optical and assumes 100% IQE in the active layers to calculate photocurrents.

The aging experiments are done in a self-made setup which has been built in cooperation with Heliatek GmbH (Dresden, Germany). This setup provides a long-term stable system for heating, illumination, and measurement of multiple samples. During the aging measurements, the sample was constantly illuminated and held at 50°C . We can apply different illumination intensities provided by two high-power LEDs. Thus, it is possible to exchange the illumination color between different experiments. White LEDs (Philipps Lumileds, LUXEON L XK2-PWC4-0220) with a continuous emission spectrum from 400–700 nm deliver up to 1000 mW/cm^2 , which equals

the intensity of ten suns, on the area of our devices (6.18 mm^2). The intensity values are directly extracted from the short circuit current of each device, as the current at 100 mW/cm^2 is known. Light illumination intensity for the aging experiments in the current study is at 999 mW/cm^2 .

III. RESULTS

A. Basic characterization

The optical constants n and κ , determined from measurements of transmittance and reflectance of thin films on glass as described elsewhere,¹³ are shown in Fig. 1(left), with the molecular structure shown on the right. The molecule consists of a diindenoperylene core with four phenyl rings and four propyl chains as substituents; calculations suggest a three-dimensional structure of the molecule, with the phenyl rings being orthogonal to the central diindenoperylene core.¹¹

The spectrum of the extinction coefficient κ represents the absorption peaks of P4-Ph4-DIP at 493 nm, 525 nm and 568 nm. The extinction maxima of P4-Ph4-DIP are between those of C_{60} (<450 nm) and ZnPc (peaks at 630 and 704 nm), such that this perylene derivative fills the optical gap between these two materials.

The perylene compound is examined by cyclic voltammetry (CV) concerning the electrochemical behavior using CH_2Cl_2 as solvent and tetrabutylammonium hexafluorophosphate (TBAPF, 0.1 mol L^{-1}) as electrolyte with a scan rate of 100 mV s^{-1} . The frontier orbital energy levels are calculated from the first and second reduction potential,¹⁴ determined with respect to ferrocene.¹⁵ The calculated lowest unoccupied molecular orbital (LUMO) and highest occupied molecular orbital (HOMO) energy levels are -3.16 eV and -5.34 eV , respectively.

Photoelectron spectroscopy measurements of evaporated thin films on amorphous Au foil place the ionization potential (IP) at 5.5 eV, which is in good agreement with the CV values and will be used in the remainder of this work.

The LUMO is verified with the empirical formula described by Djurovich.¹⁶ The optical gap of P4-Ph4-DIP is determined from absorption measurements to be $E_{\text{opt}} = 2.06 \text{ eV}$. The electrical band gap E_{g}^t can be calculated with

$$E_{\text{g}}^t = (1.39 \pm 0.15)E_{\text{opt}} - (0.46 \pm 0.38) \text{ eV}, \quad (1)$$

as described elsewhere.¹⁶ We obtain $E_{\text{g}}^t = (2.4 \pm 0.7) \text{ eV}$, resulting in a value for the electron affinity of $(3.1 \pm 0.7) \text{ eV}$, which fits well to the CV data.

To study basic film morphology, 100 nm thick intrinsic thin films of P4-Ph4-DIP are evaporated onto C_{60} -coated glass substrates and then studied by atomic force microscopy (AFM). C_{60} is chosen as underlayer to emulate realistic conditions of a complete SMOSC, where the donor is embedded between C_{60} and hole transport layer (HTL). Identical samples are prepared on heated substrates ($T_{\text{sub}} = 100^\circ\text{C}$) to probe for structural differences related to substrate temperature.¹⁷ X-ray diffraction (XRD) is employed to characterize possible crystallinity.

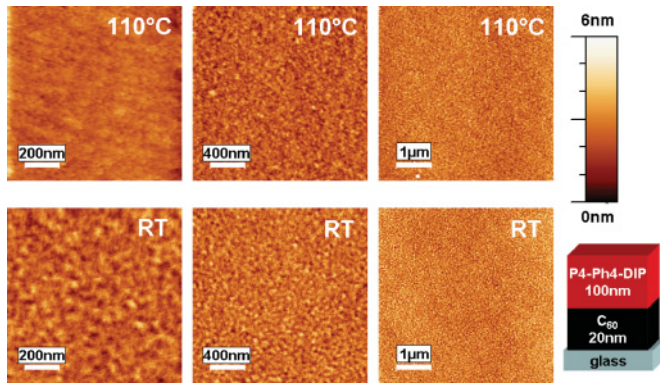


FIG. 2. (Color online) AFM micrographs of intrinsic P4-Ph4-DIP on C_{60} -coated glass, deposited with the substrate heated to 110°C (top row), or unheated (bottom row). Extremely smooth layers are observed, with the highest peaks being typically smaller than 6 nm. The images were taken from different areas. Small picture bottom right: sample stack.

The root mean square roughnesses R_{rms} of the different samples are evaluated with

$$R_{\text{rms}} = \sqrt{\frac{1}{MN} \sum_{m=1}^M \sum_{n=1}^N [z(x_m, y_n) - \langle z \rangle]^2}. \quad (2)$$

Here, M and N are integers and correspond to the number of data points; z is the height measured at each coordinate (x, y) . All samples shown in Fig. 2 exhibit low roughness (the z scale is 6 nm), and no large peaks, protrusions, or structures are visible, independent of the substrate temperature. We find very low roughnesses for the samples on unheated substrates, with $R_{\text{rms}} = (0.64 \pm 0.04)$ nm. However, this is even further reduced in the samples deposited on heated substrates, where the roughness decreases to $R_{\text{rms}} = (0.55 \pm 0.04)$ nm. This is in strong contrast to findings of, e.g., dicyanovinyl-oligothiophenes (DCV6T) mixed with C_{60} , where elevated substrate temperatures induce structures and large grains, and film roughness increases fivefold upon heating.¹⁸

Considering that scanning electron micrographs do not resolve any features, and that XRD patterns exhibit no Bragg reflections that would indicate a crystalline phase (data not shown), we conclude that P4-Ph4-DIP forms amorphous layers. Substrate heating, which can lead to considerable crystallization in other materials like ZnPc: C_{60} or DCV6T: C_{60} heterojunctions,^{18,19} leads to additional reorganization and smoothing of P4-Ph4-DIP molecules within the layer, and does not induce a phase change.

B. Organic solar cells

1. Solar cell performance: Current voltage properties

Organic solar cells are made to test the properties of P4-Ph4-DIP as donor. The devices have $n-i-p$ structure, with the absorber layers embedded between n -doped and p -doped layers.²⁰ As donor, P4-Ph4-DIP is used in a FHJ with C_{60} as acceptor. We expect that the energy alignment of P4-Ph4-DIP to the hole transport material 9,9-bis[4-(N,N -bis-biphenyl-4-yl-amino)phenyl]-9H-fluorene (BPAPF),²¹ which has an IP of 5.6 eV, provides excellent hole extraction via p -doped ZnPc

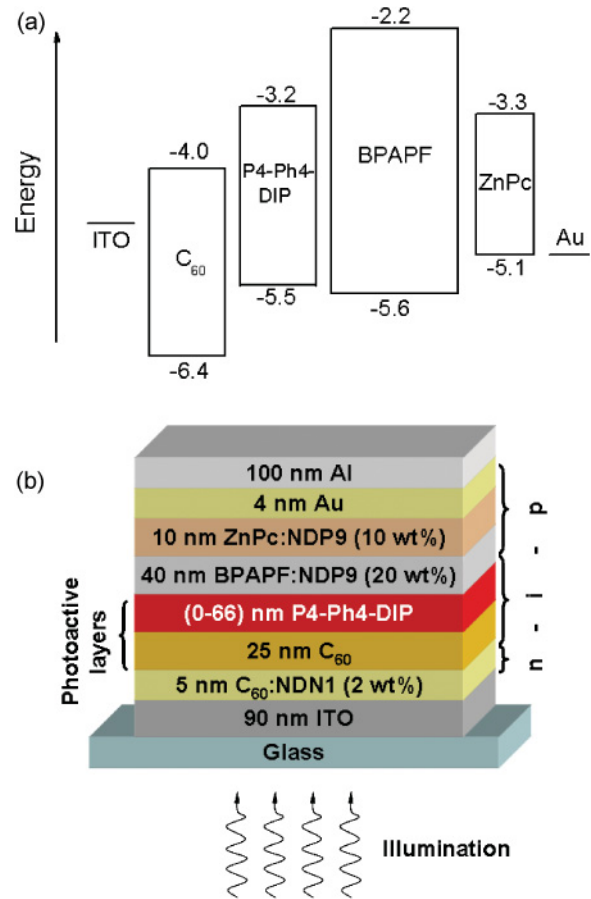


FIG. 3. (Color online) (a) Schematic energy levels and (b) layer stack of the investigated SMOSC.

toward a metal electrode. Electron extraction is via C_{60} toward ITO. The energy levels are depicted schematically in Fig. 3(a), with the corresponding device layer stack shown in Fig. 3(b).

To probe the influence of donor thickness t_d , 23 device configurations are created under identical conditions, with t_d between 0–66 nm. For each t_d , four identical solar cells are made to ensure reliable and representative measurement results.

The characteristic parameters open circuit voltage V_{OC} , fill factor FF, short-circuit current density J_{SC} , and efficiency η of SMOSC employing P4-Ph4-DIP as donor in FHJ are listed in Table I, with the corresponding $J(V)$ data shown in Fig. 4(top). A device without perylene donor is given as reference, where the FHJ is between BPAPF and C_{60} . The original results for J_{SC} from the $J(V)$ measurements are given in the table, together with the corresponding mismatch-corrected intensities and efficiencies. All $J(V)$ curves shown in Fig. 4(top) are the original measurement data.

The values of the short-circuit current density that are discussed in the text and compared in the other figures correspond to $J_{\text{SC, norm}}$, i.e., the short-circuit current density normalized to 100 mW/cm^2 . This allows for direct comparison of different samples that were measured at different intensities. For all samples containing P4-Ph4-DIP as donor, the average illumination intensity is $(113 \pm 2.5) \text{ mW/cm}^2$, and the spectral mismatch factor varies by less than 2%, such that the normalization is a valid basis for discussion.

TABLE I. Parameters of SMOSC with P4-Ph4-DIP FHJ structures. Illumination intensities and power conversion efficiencies are corrected for spectral mismatch. The donor thickness is denoted with t_d ; the $J_{SC, \text{norm}}$ values are the short-circuit current densities, normalized to 100 mW/cm^2 illumination.

#	t_d nm	J_{SC} mA/cm ²	$J_{SC, \text{norm}}$ mA/cm ²	V_{OC} V	FF %	I^* mW/cm ²	Sat	η^* %
A	0	1.95	1.81	0.67	63.4	107.5	1.25	0.8 ± 0.05
B	9	2.97	2.62	0.98	75.7	113.5	1.08	1.9 ± 0.1
C	15	2.95	2.58	0.99	75.7	114.2	1.06	1.8 ± 0.1
D	27	2.59	2.24	0.99	73.7	115.5	1.04	1.6 ± 0.1
E	45	1.85	1.61	0.99	66.8	115.2	1.04	1.1 ± 0.05
F	63	1.34	1.20	0.98	59.8	111.8	1.05	0.7 ± 0.05

The V_{OC} data exhibit high voltages of close to 1 V and document that this combination of fullerene and perylene derivative is excellent in terms of energy-level alignment. The maximum open circuit voltage depends on the highest occupied and lowest unoccupied molecular orbitals (HOMO and LUMO) of donor and acceptor. We define

$$E_{g, \text{effective}} = |\text{HOMO}_{\text{donor}}| - |\text{LUMO}_{\text{acceptor}}| \quad (3)$$

as an effective donor-acceptor band gap. Several studies document a linear proportionality of V_{OC} and $E_{g, \text{effective}}$,^{22–31} with a typical offset voltage of 0.3 V by which V_{OC} is smaller than the effective band gap. Cheyns *et al.* calculated for bilayer devices or flat heterojunctions that

$$q V_{OC} = E_{g, \text{effective}} - k T \ln \frac{N_D N_A}{p_i n_i} + \Delta_{\text{low}}(F), \quad (4)$$

with the elementary charge q and Boltzmann's constant k .³² N_D and N_A are the densities of state of donor (HOMO) and acceptor (LUMO), respectively, and p_i and n_i the carrier concentrations of holes and electrons at the donor-acceptor heterointerface. Here, $\Delta_{\text{low}}(F)$ represents field-dependent barrier lowering between electrical contacts and donor or acceptor layer.

The LUMO of C_{60} has been reported to be $\approx -4 \text{ eV}$.^{33,34} This means that the highest possible $V_{OC, \text{max}}$ with P4-Ph4-DIP would be $\approx 1.5 \text{ V}$ if there were no losses of any kind. Experimentally, voltages of almost 1 V are observed, indicating that $\approx 0.5 \text{ V}$ are lost. This compares favourably to ZnPc: C_{60} heterojunctions, where the HOMO of ZnPc (placed at -5.1 to -5.28 eV ^{35,36}) limits $V_{OC, \text{max}} < 1.1$ – 1.28 V , and experimentally, usually $\approx 0.5 \pm 0.05 \text{ V}$ are obtained,^{3–9} indicating a higher loss for ZnPc: C_{60} -based devices. The voltages reported in this contribution correlate to the current density; with an increase of J_{SC} from 1.2 mA/cm^2 to 2.6 mA/cm^2 , V_{OC} increases from $\approx 0.976 \text{ V}$ to 0.993 V . We attribute this to higher quasi-Fermi level splitting due to higher charge carrier densities in SMOSC with high J_{SC} . However, this influence is rather small, and the effective gap is expected to be the most decisive influence on V_{OC} .

The $J(V)$ curves in Fig. 4 document extremely high FF in combination with excellent saturation in reverse direction; ratios of $J(-1 \text{ V})/J(0 \text{ V})$ in the range of 1.08 to 1.04 are observed, with lower ratios, i.e., better saturation values being found for larger P4-Ph4-DIP thicknesses. We attribute this

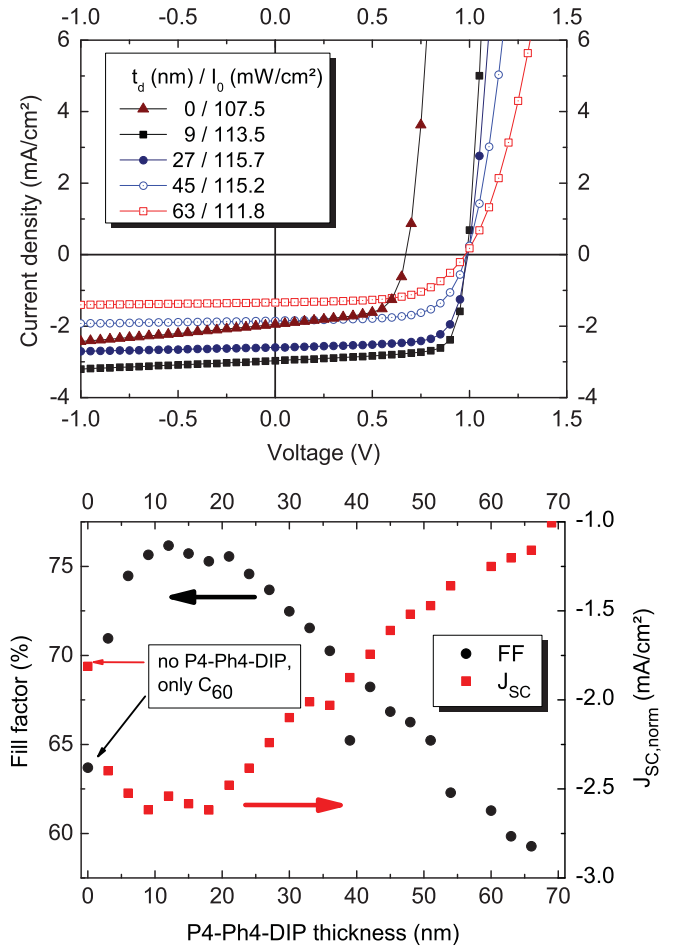


FIG. 4. (Color online) Top: $J(V)$ spectra of FHJ devices with different thicknesses of P4-Ph4-DIP. All SMOSC exhibit very high FF and excellent saturation in reverse bias, with FF decreasing for higher thicknesses. J_{SC} drops, but V_{OC} is not strongly influenced by the P4-Ph4-DIP thickness. Bottom: Fill factor FF (left axis, squares) and normalized short-circuit current density $J_{SC, \text{norm}}$ (right axis, circles) of SMOSC having FHJ with different t_d . The data points at the far left represent a reference sample with only C_{60} as absorber.

behavior to a highly efficient transport of electrons and holes once the corresponding excitons have been dissociated, with a low field dependency of exciton dissociation and charge carrier extraction.

The largest influence of t_d is observed in measurements of FF and $J(V)$, as shown in Fig. 4(bottom). The photocurrent is determined to be $J_{SC, \text{norm}} = 1.81 \text{ mA/cm}^2$ if only C_{60} is present as absorber. Upon addition of perylene absorber layers, the current increases to a peak of 2.62 mA/cm^2 at 18 nm P4-Ph4-DIP thickness, with highest currents being observed in samples with 9–21 nm thickness. For larger thicknesses, the current then decreases, dropping to 1.16 mA/cm^2 at 66 nm absorber thickness. We attribute this to a low exciton diffusion length, as will be explained further below.

Exhibiting a similar behavior like the photocurrent, the best fill factors are observed at 9–21 nm thickness, with a peak of 76.2% at 12 nm absorber thickness. To our knowledge, this is currently the highest value published in the field of organic photovoltaics. The high FF are attributed to very

efficient separation of photogenerated excitons at the interface P4-Ph4-DIP to C_{60} , followed by efficient transport of holes toward the HTL. The fill factor decreases only at higher donor thicknesses; however, even at thicknesses of over 60 nm, the FF remains $>59\%$, which competes with the best ZnPc: C_{60} devices.

2. Solar cell performance: EQE

The external quantum efficiency of the complete series of SMOSC with different i-P4-Ph4-DIP thicknesses (0–66 nm) is shown in Fig. 5. The EQE spectra exhibit a characteristic peak at 350 nm, corresponding to the first absorption maximum of C_{60} , with EQE between 15–20%. The actual contribution of this maximum to the total device photocurrent is relatively small, since the intensity of the AM 1.5G spectrum is low at $\lambda < 400$ nm. The peak height varies with the perylene layer thickness, which is attributed to interference effects of the optical field in the device.

The fullerene's second maximum, situated at 450 nm, is visible as shoulder of a convolution of three peaks and two shoulders between 450–600 nm, one of which originates from the fullerene and four of which represent the perylene. The highest EQE of 23% at 450 nm is observed at 0–3 nm P4-Ph4-DIP thickness, i.e., when the photocurrent originates solely ($t_d = 0$ nm) or mostly ($t_d = 3$ nm) from the C_{60} . With increasing perylene thickness, the EQE of C_{60} at 450 nm decreases, dropping to $<5\%$ for thicknesses >57 nm. This development is caused by the shift of the optical field maximum away from the donor-acceptor interface further into the donor layer: the lower field intensity in the fullerene reduces charge carrier generation in the acceptor, as will be shown below in Fig. 6.

The EQE of P4-Ph4-DIP, represented by the peaks at 525 nm and 567 nm, reaches highest values of $>20\%$ at $t_d < 20$ nm and then decreases steadily with increasing t_d .

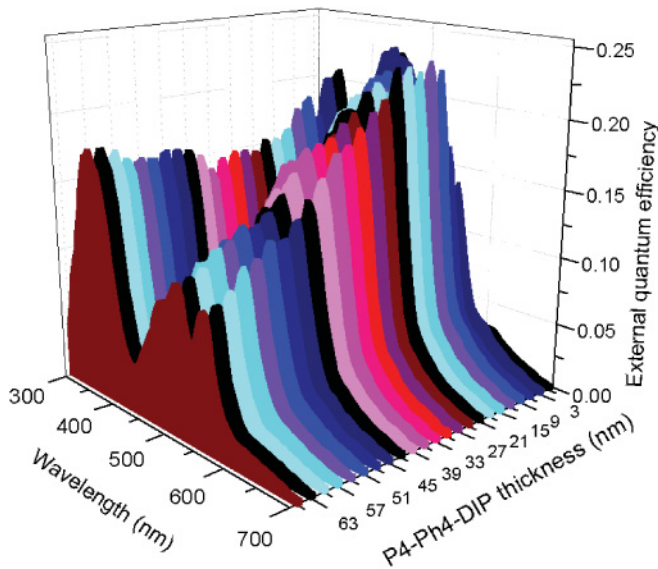


FIG. 5. (Color online) EQE spectra of FHJ devices with different thicknesses of P4-Ph4-DIP. With increasing t_d , we observe a decrease of EQE of C_{60} at the material's main peak at 450 nm, a drop in EQE of the green donor. The peak EQE of P4-Ph4-DIP is observed at $t_d = 9, \dots, 18$ nm.

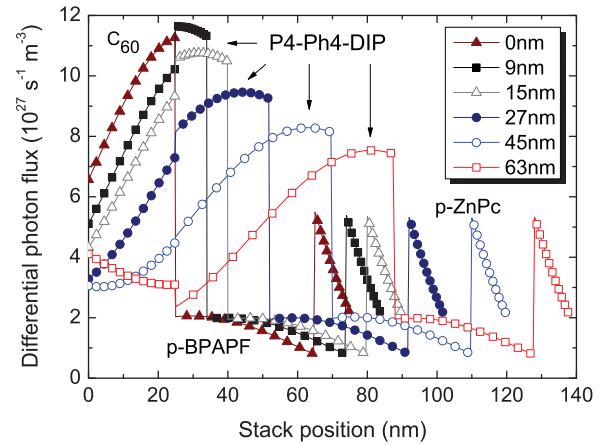


FIG. 6. (Color online) Differential photon flux per unit propagation length of FHJ devices with different thicknesses of P4-Ph4-DIP. The simulations document the shift of the optical-field maximum further into the intrinsic P4-Ph4-DIP and away from the donor-acceptor interface with increasing t_d . The metal contacts are omitted for better visibility.

This corresponds to the earlier observations of decreasing $J_{SC, norm}$. A possible reason for the drop of photocurrent at higher donor thickness may be a small exciton diffusion length L_D . High $L_D > 100$ nm has been reported for pure crystals of unsubstituted diindenoperylene (DIP),³⁷ determined by the method described by Ghosh and Feng.³⁸ However, this is controversially discussed,³⁹ and L_D between 17–22 nm have also been reported for the same material, depending on the orientation of crystallinity.³⁹ In the current case, the phenyl and propyl substituents of P4-Ph4-DIP may prevent planarity and result in a three-dimensional molecular structure,¹¹ resulting in the growth of amorphous films. This leads to lower packing density and reduced molecular orbital overlap, reducing L_D far below that of pure DIP.

To differentiate between optical and electrical effects, and to probe the influences of interference effects on EQE and photocurrent, we perform calculations of the differential photon flux per unit propagation length under AM 1.5G. This is achieved by using a numerical algorithm⁴⁰ based on the transfer-matrix approach and Poynting vector computations.⁴¹ A model validation and an application to other SMOSC systems are published elsewhere.^{42,43}

The results are depicted in Fig. 6. In the graph, ITO and n-doped C_{60} are omitted for better visibility since they do not contribute to photocurrent. The metal top contact (Au and Al) is omitted as well for better visibility of the active organic layers.

The figure illustrates that the p-doped HTL layers lead to slight parasitic absorption. However, the BPAPF absorbs only weakly due to the wide band gap, and ZnPc is close enough to the field node provided by the metal back contact such that the optical field intensity is low. The low absorption of the p-doped HTL is expected to provide no contribution to the photocurrent since the dopants act as quenching sites. The photon flux and possible contribution of the C_{60} layer decrease with increasing t_d , confirming the decreasing peak at 450 nm in the EQE data.

For P4-Ph4-DIP, it is visible that the highest photon flux is encountered directly next to the donor-acceptor heterointerface

for $t_d = 3$ nm. With increasing t_d , the field maximum in the donor layer shifts away from the donor-acceptor heterojunction toward the metal top contact; while the total integrated flux (and hence photocurrent) of the P4-Ph4-DIP increases with increasing t_d , the contribution of the volume close to the interface is lowered. This is especially pronounced in the 63 nm perylene layer, where the maximum is 50 nm away from the C_{60} :P4-Ph4-DIP interface, and the photon flux close to the interface is smaller by a factor of four compared to the SMOSC with 9 or 15 nm.

The development of differential photon flux of the intrinsic C_{60} layer is explained by the interference/optical field distribution: for thin P4-Ph4-DIP layers, there is a high field intensity in the blue range (where C_{60} absorbs) close to the donor-acceptor interface. With higher P4-Ph4-DIP thickness, this becomes weaker. There is a minimum in the C_{60} photon flux at 45 nm thickness at stack position 5 nm. For higher P4-Ph4-DIP thickness, this minimum moves toward the middle of the intrinsic C_{60} layer, and then moves toward the donor-acceptor interface for even higher P4-Ph4-DIP thicknesses.

In summary, we conclude that a thick perylene layer would lead to higher photocurrents even for $t_d > 45$ nm if L_D were high enough, and the calculations show that optical effects are not the major limiting factor for device performance.

3. Determination of the exciton diffusion length

The exciton diffusion length L_D is a crucial parameter to evaluate the suitability of a given material for photovoltaic applications. The two methods that are commonly used to determine L_D are thickness-dependent or spectrally resolved photoluminescence (PL) quenching, or the photoresponse of a metal-organic Schottky diode, as described by Ghosh and Feng.³⁸ Both methods can be performed on relatively simple samples (e.g., only two or three layers are necessary), but have their shortcomings.

PL quenching leads to uncertainties if the film thickness of the investigated material is in the range of L_D ;⁴⁴ interference effects of probed layer and quenching layer may obscure and dominate the measurement,⁴⁵ and morphological effects of thin layers may pose additional problems.^{39,45} In metal-organic Schottky diodes, on the other hand, interactions of metal and organic layers other than excitonic effects may play an important role, but may not be properly considered. Examples are interpenetration of metal atoms into organic layers,^{46,47} plasmonic effects, long-range energy transfer from the metal layer to organic molecules, and interference effects.⁴⁸

For a correct determination of L_D of a material that is to be used as solar cell absorber, it is reasonable to investigate this property in realistic conditions, i.e., with the material being utilized in an actual solar cell. Here, further optical and electrical calculations are carried out to gain information about L_D of P4-Ph4-DIP from devices. For this purpose, the experimentally measured EQE spectra of all devices are used to determine short-circuit photocurrent densities $J_{SC,EQE}$ for all donor thicknesses, which are varied in 3 nm steps from 0–66 nm. This provides an additional cross-check of the measured values of $J_{SC,norm}$, and it is found that $J_{SC,EQE}$ and $J_{SC,norm}$ are in good agreement (see inset of Fig. 7).

The same devices are then simulated, with the P4-Ph4-DIP layer of each sample split into n finite elements of 3 nm thickness (since $t_d = 0, \dots, 66$ nm, we have $n = 0, \dots, 22$). The software calculates $J_{SC,n}$ for each 3-nm element, assuming AM 1.5G illumination and 100% IQE. This takes the optical field distribution into consideration and allows to investigate in detail the contribution of each 3-nm-slice to the total device photocurrent $J_{SC,norm}$.

By correlating experimental [from EQE and $J(V)$ spectra] and calculated photocurrents, it is possible to find weighting factors that reflect the lower contributions from slices farther away from the donor-acceptor heterointerface, and represent electrical losses of excitons that are generated in the donor layer, but cannot reach the interface for dissociation.

The total simulated photocurrent $J_{SC,total}$ for each t_d can be calculated for each of the 22 device configurations by

$$J_{SC,total}(t_d) = w_{n,C60} J_{SC,C60}(t_d) + \sum_{i=0}^n w_n J_{SC,n}(t_d), \quad (5)$$

with n being an integer ($n = \frac{t_d}{3}$). The contribution of the n th slice of P4-Ph4-DIP is calculated by the simulated current $J_{SC,n}$ of each slice, multiplied by the weighting factor w_n .

Here, $J_{SC,C60}$ represents the contribution of the 25 nm thick layer of intrinsic C_{60} . The weighting factor $w_{n,C60}$ to calculate the contribution of the intrinsic fullerene layer to total device photocurrent is determined from the reference device without perylene donor and is then kept constant for all n . However, the photocurrent $J_{SC,C60}$ is recalculated for each t_d to correctly consider the influence of interference effects.

Figure 7 shows the weighting factors w_n of each slice, plotted vs. the total donor thickness, counting from the heterointerface. The first 3 nm of the diindenoperylene derivative are assumed to contribute with 100% efficiency (i.e., all excitons are dissociated and the resulting charge carriers collected), the second 3 nm with 64%, the third 3 nm of each device with 42%, etc. The weighting factors, which are found empirically to follow an exponential decay, lead to

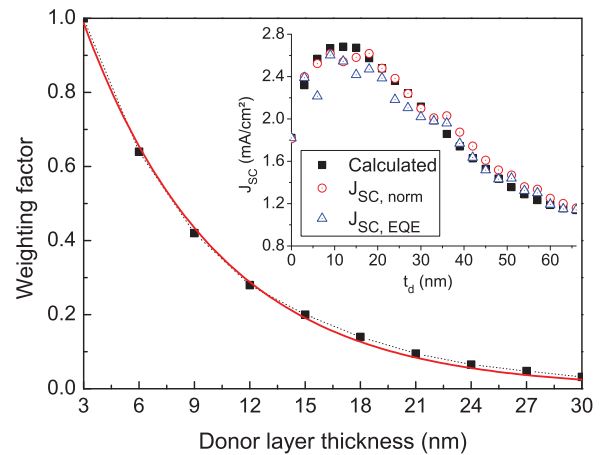


FIG. 7. (Color online) Squares: calculated weighting factors w_n with which the n th 3-nm-thick slice contributes to the photocurrent. Thick line: exponential fit [Eq. (5)]. Inset: short-circuit current densities at 100 mW/cm² of FHJ devices with different t_d , determined by experiment [EQE setup and $J(V)$ measurements] and optical calculation.

excellent agreement of experiment and calculation; the data suggest that there is only little contribution (<20%) from the P4-Ph4-DIP volume that is more than 15 nm away from the separating donor-acceptor interface. The w_n follow the empirical relationship

$$w_n = a e^{bt_d} = a e^{b(3n)}, \quad (6)$$

with $a = 1.49 \pm 0.03$ and $b = -0.14 \pm 0.003$. With this formula, the half-maximum of the weighting factors, i.e., the thickness after which >50% of the excitons are lost, can be determined to be $t_d \approx 8$ nm. The inset of Fig. 7 shows the photocurrents as determined by the EQE and $J(V)$ measurements, and the calculated $J_{SC,total}$ as determined by Eqs. (5) and (6). An excellent agreement of measured and calculated values is seen for all t_d values.

To verify our optically determined L_D , we have also performed numerical calculations based on the continuity equation for excitons. The good saturation behavior (saturation ratio always <1.1) allows to utilize $J_{SC,norm}$ of the SMOSC as best approximation for the photocurrent. At this point we assume the field dependent exciton dissociation efficiency and charge carrier collection efficiency to be unity. The small increase of (absolute) current density under negative bias seems to be dominated by a photoshunt effect due to its linearity, showing no saturation tendency. When the absolute spectrum of the illumination light is known, J_{SC} is sufficient to estimate the exciton diffusion length L_D . Therefore the following continuity equation for excitons is used:

$$\frac{\partial s}{\partial t} = G_{opt} - \frac{s}{\tau} - R_{sep} + \frac{L_D^2}{\tau} \frac{\partial^2 s}{\partial x^2}, \quad (7)$$

where the diffusion constant D in Eq. (7) is represented by L_D and lifetime τ as in

$$D = \frac{L_D^2}{\tau}. \quad (8)$$

The change of exciton density s within the layers is governed by an optical generation term G_{opt} , a relaxation term with a lifetime τ and an expression for the diffusion. At the donor-acceptor interface there is an additional drain, i.e., the separation R_{sep} followed by a dissociation into free charge carriers. The absorbed photon flux is used for the generation rate, obtained from a coherent simulation of the stack via a transfer matrix formalism⁴⁹ with the optical constants of the materials and the illumination spectrum as input. As long as $\tau \ll \frac{1}{r_{sep}}$ (with $R_{sep} = s_{interface} r_{sep}$), the solution of Eq. (7) is independent of τ and R_{sep} . This assumption is justified, because the charge transfer to the acceptor C_{60} is known to happen in the femtosecond range,^{50,51} whereas exciton lifetimes are at least in the range of ns. Remaining is only the exciton diffusion length L_D as parameter.

We solve Eq. (7) numerically using a self-made solar-cell simulation software. The employed algorithm is based on finite differences and calculates the steady-state solution of Eq. (7). We compare the results to the measured $J_{SC,norm}$ and the current calculated for AM1.5G from the measured EQE, i.e., $J_{SC,EQE}$, assuming a linear superposition of the current contribution of all wavelengths. Figure 8 shows the results. Both the calculated AM1.5G photocurrent from measured EQE data and the measured $J_{SC,norm}$ under a simulated spectrum are

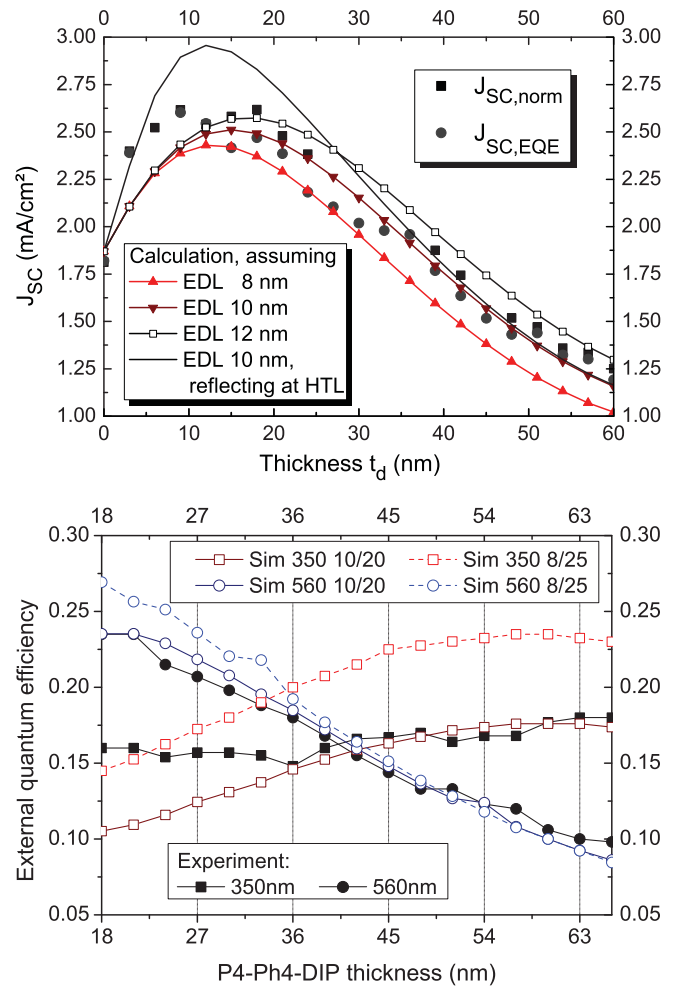


FIG. 8. (Color online) Top: Short circuit current densities of FHJ devices with different t_d , determined by experiment [EQE setup and $J(V)$ measurements] and calculation. The best reproduction of the experimental values is obtained with $L_D = 10$ nm. Bottom: Simulated EQE at the absorption peaks of C_{60} (350 nm) and P4-Ph4-DIP (560 nm), determined experimentally (full symbols) or numerically (empty symbols). Good agreement is reached with set **B**, corresponding to $L_D = 10$ nm for P4-Ph4-DIP and $L_D = 20$ nm for C_{60} .

well reproduced by the simulation with an exciton diffusion length of $L_D = 10$ nm for P4-Ph4-DIP and 20 nm for C_{60} . The value for C_{60} is reasonable and is within the range of values reported in literature (ranging from 8–40 nm^{49,52}).

For thin layers ($t_d \leq L_D$) the interface between donor and HTL gets important. As seen from Fig. 8(top), the best fit to the experimental data is obtained if one assumes exciton quenching at the interface to the doped HTL, instead of exciton reflection. This exciton quenching makes the estimation of the precise diffusion length in C_{60} for the sample with 0 nm P4-Ph4-DIP difficult.

Furthermore, data points for thicknesses $t_d < 9$ nm have to be taken with care, because in this thickness range effects, like inhomogeneous layer coverage, can play a role. To give an idea how sensitive to L_D the current is and how strongly the boundary condition at the donor/HTL interface influences the results, there are three additional curves in Fig. 8, representing

$L_D = 8$ nm (triangles), $L_D = 12$ nm (empty squares), and $L_D = 10$ nm with exciton reflection at the HTL (line without symbols).

Assuming exciton reflection at the HTL, J_{SC} is overestimated for $t_d < 30$ nm. 12 nm L_D is too high because the position of the maximum of J_{SC} is found at $t_d = 18$ nm, which does not correspond to the experimental findings, and because the currents obtained at $t_d > 18$ nm are too high.

For thick layers, only the exciton diffusion lengths of C_{60} and P4-Ph4-DIP dominate the curve. Hence, a small exciton diffusion length in P4-Ph4-DIP could in principle be compensated by a higher value for C_{60} , resulting in the same total photocurrent. Hence, the shape of the 8 nm curve seems quite reasonable, and could be shifted up to match the experimental data if a higher-exciton diffusion length of C_{60} were assumed (e.g., 25 nm). Thus, verification is required if the parameter set of 10/20 nm is correct, or if 8/25 nm could reproduce the experimental findings just as well. To check if we have found the correct contribution of C_{60} and P4-Ph4-DIP to the photocurrent, i.e., the correct exciton diffusion lengths, we simulate the EQE as well. Two parameter sets are used: L_D of P4-Ph4-DIP of 8 nm with L_D of C_{60} of 25 nm (denoted as set **A**), and a second set **B** with 10 nm and 20 nm, respectively. Both sets yield qualitatively acceptable fits and deliver approximately the same total photocurrents.

We now compare in more detail the maxima of the peaks in the EQE at 560–570 nm (P4-Ph4-DIP absorption) and at 350 nm (mostly C_{60}) for larger layer thicknesses, where only the exciton diffusion length limits the current. The results are shown in the bottom part of Fig. 8, where the simulation is done using an arbitrary fixed intensity. Hence, the simulation data for the two peaks of set **B** are scaled with one factor for good agreement with experimental data and **A** is scaled with another factor, respectively. With this method, the ratio between the 350 nm and the 560 nm peaks is conserved and can be compared. It is obvious that an exciton diffusion length of 25 nm for C_{60} (set **A**) overestimates the contribution of C_{60} and distorts the peak ratio of C_{60} and P4-Ph4-DIP. Set **B** describes the P4-Ph4-DIP peak (560 nm) very well over the whole thickness range and the C_{60} peak for higher thicknesses as well.

The fit over a thickness range of 0–66 nm yields a very reliable estimate of $L_D = 10$ nm, which is verified by comparison with the EQE. Combined with the electrical simulations shown in Fig. 8(top) and the optical simulations shown in Fig. 7, we conclude that P4-Ph4-DIP has an exciton diffusion length of 9 ± 1 nm. This is significantly smaller than any value that is given for DIP in the literature, and a strong document of the influence of the side groups on electrical properties.

4. Aging

Finally, to characterize device stability, solar cells with 12 nm P4-Ph4-DIP are tested for degradation under accelerated aging. As light illumination, white LEDs with a very high intensity of ≈ 999 mW/cm² are used, with the devices held at 50 °C. The resulting characteristics are shown in Fig. 9. The initial absolute values are $J_{SC} = 25.8$ mA/cm², FF = 62.9%, and $V_{OC} = 1.02$ V. An absolute initial η is not given since the spectral mismatch of the aging setup is not known.

The open circuit voltage remains almost unchanged throughout the measurement, decreasing by only 2%. Within

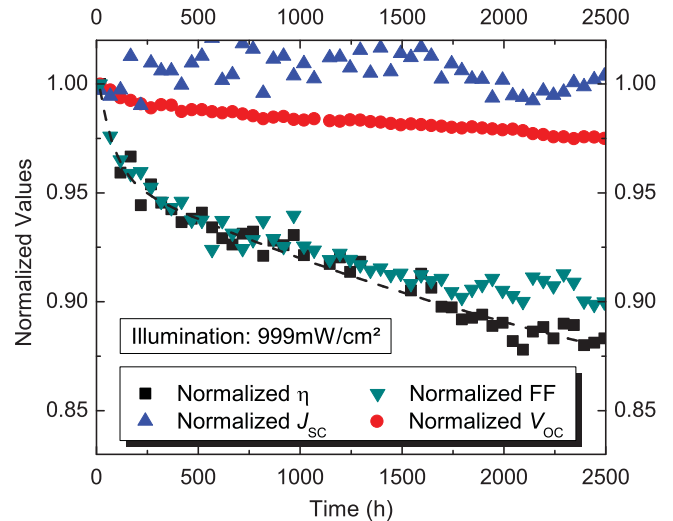


FIG. 9. (Color online) Aging of a FHJ device with 12 nm of P4-Ph4-DIP as donor reveals high device stability.

experimental scatter, J_{SC} remains at the initial value during the experiment. Degradation is mainly mediated by losses of FF, which decreases by relative 10% during intense illumination of 2500 h at ≈ 10 suns. The combination of losses of voltage and fill factor leads to a relative loss of power conversion efficiency of 12%. We hence consider P4-Ph4-DIP an extremely stable material. Extrapolation from an exponential fit (dashed line in Fig. 9) suggests that the devices maintain $>80\%$ of their initial efficiency even after 20 000 h of operation.

IV. CONCLUSION

A diindenoperylene derivative with phenyl and propyl substituents is introduced as alternative donor material for small molecule organic solar cells. We show that extremely high fill factors of $>76\%$ can be obtained, and due to the very favorable energy level alignment to C_{60} , high voltages close to $V_{OC} = 1$ V are observed.

However, the power conversion efficiency is limited to $\eta < 2\%$ by the photocurrents, which are well below 3 mA/cm². We explain this with a small exciton diffusion length L_D . By employing optical and electrical calculations, we find $L_D = 9 \pm 1$ nm for the donor P4-Ph4-DIP. However, the bulk heterojunction concept may help improve this deficit, as has been shown for a similar derivative where higher photocurrents were achieved.⁵³

The devices exhibit excellent stability, with only 12% degradation after 2500 h at high-intensity illumination of 10 suns.

ACKNOWLEDGMENTS

The current work is supported by the Bundesministerium für Bildung und Forschung in the framework of the InnoProfile project (03IP602) and OPA project (13N9872). W.T. thanks the Reiner Lemoine foundation for funding.

- *moritz.riede@iapp.de; [http://www.iapp.de]
- ¹8.3% efficient SMOSC on 1.1 cm² area, made by Heliatek/IAPP, certified at Fraunhofer ISE (Freiburg) (2010).
- ²8.3% efficient polymer device made by Konarka in 2010, certified by NREL. See the newsroom of [http://www.konarka.com/] (accessed Dec. 20, 2010).
- ³J. Meiss, N. Allinger, C. Falkenberg, K. Leo, and M. K. Riede, *Proc. SPIE* **7416**, 741603 (2009).
- ⁴T. Taima, J. Sakai, T. Yamanari, and K. Saito, *Sol. Energy Mater. Sol. Cells* **93**, 742 (2009).
- ⁵J. Drechsel, A. Petrich, M. Koch, S. Pfuetzner, R. Meerheim, S. Scholz, K. Walzer, M. Pfeiffer, and K. Leo, *SID Symposium Digest of Technical Papers* **37**, 1692 (2006).
- ⁶R. Lessmann, Z. Hong, S. Scholz, B. Maennig, M. K. Riede, and K. Leo, *Organic Electronics* **11**, 539 (2010).
- ⁷M. Egginger, R. Koeppel, F. Meghdadi, P. A. Troshin, R. N. Lyubovskaya, D. Meissner, and N. S. Sariciftci, *Proc. SPIE* **6192**, 61921Y-1 (2006).
- ⁸G. Dennler, H.-J. Prall, R. Koeppel, M. Egginger, R. Autengruber, and N. S. Sariciftci, *Appl. Phys. Lett.* **89**, 073502 (2006).
- ⁹B. Yu, L. Huang, H. Wang, and D. Yan, *Adv. Mater.* **22**, 1017 (2010).
- ¹⁰M. K. Riede, T. Mueller, W. Tress, R. Schueppel, and K. Leo, *Nanotechnology* **19**, 424001 (2008).
- ¹¹J. Meiss, M. Hummert, H. Ziehlke, K. Leo, and M. Riede, *Phys. Status Solidi RRL* **4**, 329 (2010).
- ¹²Used for better processibility; for organic materials with deep-lying HOMO beyond -6 eV, doping is possible by WO₃, as shown in J. Meyer, S. Hamwi, S. Schmale, T. Winkler, H.-H. Johannes, T. Riedl, and W. Kowalsky, *J. Mater. Chem.* **19**, 702 (2009).
- ¹³T. Fritz, J. Hahn, and H. Boettcher, *Thin Solid Films* **170**, 249 (1989).
- ¹⁴T. Johansson, W. Mammo, M. Svensson, M. R. Andersson, and O. Inganäs, *J. Mater. Chem.* **13**, 1316 (2003).
- ¹⁵N. G. Connelly and W. E. Geiger, *Chem. Rev.* **96**, 877 (1996).
- ¹⁶P. I. Djurovich, E. I. Mayo, S. R. Forrest, and M. E. Thompson, *Org. Electron.* **10**, 515 (2009).
- ¹⁷A. C. Dürr, B. Nickel, V. Sharma, U. Täffner, and H. Dosch, *Thin Solid Films* **503**, 127 (2006).
- ¹⁸D. Wynands, M. Levichkova, M. Riede, M. Pfeiffer, P. Baeuerle, R. Rentenberger, P. Denner, and K. Leo, *J. Appl. Phys.* **107**, 014517 (2010).
- ¹⁹S. Pfuetzner, C. Mickel, J. Jankowski, M. Hein, J. Meiss, C. Schuenemann, C. Elschner, A. Levin, B. Rellinghaus, K. Leo, and M. Riede, *Organic Electronics* **12**, 435 (2011).
- ²⁰K. Walzer, B. Maennig, M. Pfeiffer, and K. Leo, *Chem. Rev.* **107**, 1233 (2007).
- ²¹C.-W. Ko and Y.-T. Tao, *Synth. Met.* **126**, 27 (2002).
- ²²M. C. Scharber, D. Mühlbacher, M. Koppe, P. Denk, C. Waldauf, A. J. Heeger, and C. J. Brabec, *Adv. Mater.* **18**, 789 (2006).
- ²³R. Schueppel, K. Schmidt, C. L. Uhrich, K. Schulze, D. Wynands, J.-L. Brédas, E. Brier, E. Reinold, H.-B. Bu, P. Baeuerle, B. Maennig, M. Pfeiffer, and K. Leo, *Phys. Rev. B* **77**, 085311 (2008).
- ²⁴K. O. Sylvester-Hvid, *J. Phys. Chem. B* **110**, 2618 (2006).
- ²⁵K. L. Mutolo, E. I. Mayo, B. P. Rand, S. R. Forrest, and M. E. Thompson, *J. Am. Chem. Soc.* **128**, 8108 (2006).
- ²⁶C. J. Brabec, A. Cravino, D. Meissner, N. S. Sariciftci, T. Fromherz, M. T. Rispens, L. Sanchez, and J. C. Hummelen, *Adv. Funct. Mater.* **11**, 374 (2001).
- ²⁷A. Gadisa, M. Svensson, M. R. Andersson, and O. Inganäs, *Appl. Phys. Lett.* **84**, 1609 (2004).
- ²⁸B. P. Rand, D. P. Burk, and S. R. Forrest, *Phys. Rev. B* **75**, 115327 (2007).
- ²⁹T. Kietzke, D. A. M. Egbe, H.-H. Höhrhold, and D. Neher, *Macromolecules* **39**, 4018 (2006).
- ³⁰C. Deibel and V. Dyakonov, *Rep. Prog. Phys.* **73**, 096401 (2010).
- ³¹W. Tress, K. Leo, and M. Riede, *Advanced Functional Materials* (accepted).
- ³²D. Cheyns, J. Poortmans, P. Heremans, C. Deibel, S. Verlaak, B. P. Rand, and J. Genoe, *Phys. Rev. B* **77**, 165332 (2008).
- ³³J. X. Tang, Y. C. Zhou, Z. T. Lin, C. S. Lee, and S. T. Lee, *Appl. Phys. Lett.* **93**, 043512 (2008).
- ³⁴R. W. Lof, M. A. van Veenendaal, B. Koopmans, H. T. Jonkman, and G. A. Sawatzky, *Phys. Rev. Lett.* **68**, 3924 (1992).
- ³⁵A. J. Ikushima, T. Kanno, S. Yoshida, and A. Maeda, *Thin Solid Films* **273**, 35 (1996).
- ³⁶W. Gao and A. Kahn, *Appl. Phys. Lett.* **79**, 4040 (2001).
- ³⁷D. Kurrle and J. Pflaum, *Appl. Phys. Lett.* **92**, 133306 (2008).
- ³⁸A. K. Ghosh and T. Feng, *J. Appl. Phys.* **49**, 5982 (1978).
- ³⁹R. R. Lunt, N. C. Giebink, A. A. Belak, J. B. Benziger, and S. R. Forrest, *J. Appl. Phys.* **105**, 053711 (2009).
- ⁴⁰Developed by Mauro Furno at IAPP; currently unpublished.
- ⁴¹E. Centurioni, *Appl. Opt.* **44**, 7532 (2005).
- ⁴²R. Schueppel, R. Timmreck, N. Allinger, T. Mueller, M. Furno, C. Uhrich, K. Leo, and M. Riede, *J. Appl. Phys.* **107**, 044503 (2010).
- ⁴³J. Meiss, M. Furno, S. Pfuetzner, K. Leo, and M. Riede, *J. Appl. Phys.* **107**, 053117 (2010).
- ⁴⁴R. C. Powell and Z. G. Soos, *J. Lumin.* **11**, 1 (1975).
- ⁴⁵S. R. Scully and M. D. McGehee, *J. Appl. Phys.* **100**, 034907 (2006).
- ⁴⁶S. Olthof, J. Meiss, M. K. Riede, B. Lüssem, and K. Leo, *Thin Solid Films* **519**, 1872 (2011).
- ⁴⁷C. Dürr, F. Schreiber, M. Kelsch, H. D. Carstanjen, H. Dosch, and O. H. Seeck, *J. Appl. Phys.* **93**, 5201 (2003).
- ⁴⁸S. B. Rim and P. Peumans, *J. Appl. Phys.* **103**, 124515 (2008).
- ⁴⁹L. A. A. Pettersson, L. S. Roman, and O. Inganäs, *J. Appl. Phys.* **86**, 487 (1999).
- ⁵⁰J.-L. Bredas, J. E. Norton, J. Cornil, and V. Coropceanu, *Acc. Chem. Res.* **42**, 1691 (2009).
- ⁵¹P. Peumans, S. Uchida, and S. R. Forrest, *Nature (London)* **425**, 158 (2003).
- ⁵²P. Peumans, A. Yakimov, and S. R. Forrest, *J. Appl. Phys.* **93**, 3693 (2003).
- ⁵³J. Meiss, M. Hummert, A. Petrich, S. Pfuetzner, K. Leo, and M. Riede, *Sol. Energy Mater. Sol. Cells* **95**, 630 (2011).